Real-time global Raman imaging and optical manipulation of suspended carbon nanotubes

Kate Kaminska, Jacques Lefebvre, D. Guy Austing, and Paul Finnie
Institute for Microstructural Sciences, National Research Council, Building M-50, Montreal Road, Ottawa, Ontario, Canada K1A 0R6
(Received 7 February 2006; revised manuscript received 12 April 2006; published 15 June 2006)

We demonstrate confocal, direct Raman imaging of carbon nanotubes based on the detection of the *G*-band using an electron multiplying charge coupled detector. Individual carbon nanotubes and bundles of nanotubes are observed in real-time over a large area using global illumination. We use the technique to show that suspended nanotubes can be manipulated selectively with a focused laser beam and describe the relevant physical mechanisms.

DOI: 10.1103/PhysRevB.73.235410 PACS number(s): 78.67.Ch, 78.30−j, 81.07.De

I. INTRODUCTION

Refinement and innovation in imaging technologies have been essential to the development of nanostructural science and technology, particularly in the field of carbon nanotubes (CNTs). Early transmission electron microscope (TEM) images of multiwalled carbon nanotubes[1] (MWNTs) and single walled carbon nanotubes (SWNTs),[2,3] motivated a great deal of research. In addition to TEM, atomic force microscopes (AFMs) and scanning electron microscopes (SEMs) are now routinely employed in carbon nanotube analysis. More recently, confocal scanning Raman spectroscopy,[4,5] near-field scanning Raman spectroscopy,[6,7] and photoluminescence imaging[8] have been used to study SWNTs. In this paper we report real-time imaging of individual CNTs, including SWNTs, based on the detection of the Raman active *G* band [9]using an electron multiplying charge coupled detector (CCD) camera. The technique allows rapid imaging of individual CNTs and bundles over a large area. This technique is relatively easy to implement, economical, nondestructive, noninvasive, and capable of real-time imaging. We further use the technique to demonstrate that CNTs can be manipulated selectively with a focused laser beam. This method of manipulation presents opportunities for device manufacture processes such as chirality selective wiring of nanotube circuits and the construction of nanotube networks.

II. EXPERIMENTAL METHOD

A schematic of the experimental setup is shown in Fig. 1. Light from a HeNe laser (632.8 nm, 20 mW) passes through a laser line band pass filter (BP) to produce a clean single frequency beam. A lens (*L*1, 200 mm focal length) focuses the collimated laser beam in front of the microscope objective [*L*2, 50×, 0.85 numerical aperture (NA)] in order to obtain the defocused spot (20 μm diameter) necessary to produce global illumination. Alternatively, this lens can be removed resulting in a tightly focused spot (2.5 μm diameter) used to obtain local Raman spectra or to increase the laser power density. The confocal configuration is obtained by using a long wave-pass edge filter (*EF*1) as a beam splitter (641 nm edge), which reflects the laser beam and transmits the Raman scattered light from the sample. A 50/50 beam splitter (BS) sends half of the scattered light to an electron multiplying CCD camera for imaging and the other half to a grating spectrometer/CCD combination (SP) for spectroscopy. For higher sensitivity, but at the expense of simultaneity, the beam splitter can be removed for imaging, or replaced by a mirror for spectroscopy. Raman spectra of carbon nanotubes are acquired by a $\frac{1}{4}$ m single grating spectrometer (600 lines/mm) and detected by a thermoelectrically cooled CCD camera. A notch filter (NF) centered at 632.8 nm is added to reduce the Rayleigh scattered laser intensity entering the spectrometer.

Imaging of CNTs is made possible with the use of a series of filters. First, an edge pass filter (*EF*2) (641 nm edge, with optical density 9 at 632.8 nm) cuts the remaining laser intensity going through *EF*1. Second is a narrow bandpass filter (*GF*) (710 nm center wavelength, 10 nm bandwidth) selected to spectrally match the *G*-band emission for 633 nm excitation. The image is focused by *L*3 (500 mm focal length) on a thermoelectrically cooled, electron multiplying CCD camera. Ideally the filters would be placed in front of the focusing lens, but for the particular components used, the scattered background was reduced with this inverted arrangement.

This system has the capability to obtain global Raman images of carbon nanotubes with low laser power densities (20 mW on a 20 μm spot size, 60 MW/m^2) without the need for raster scanning. Even at such power densities individual CNTs can be observed in real-time with an integration time of 0.5 s per frame. Images shown in this paper were obtained with a 30 s integration time to improve the image

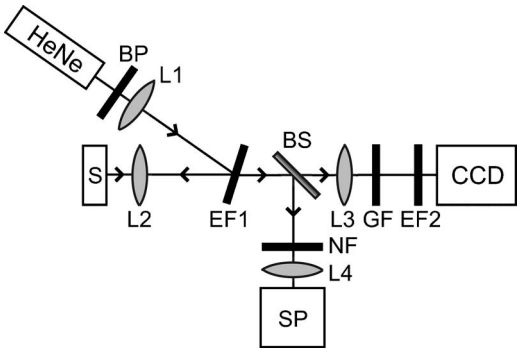

FIG. 1. Schematic of the optical setup. Imaging is performed by an electron multiplying camera (CCD) in the horizontal leg of the optical setup. Spectroscopy is performed simultaneously in the vertical leg. The various optical elements are described in the text.

 ©2006 The American Physical Society

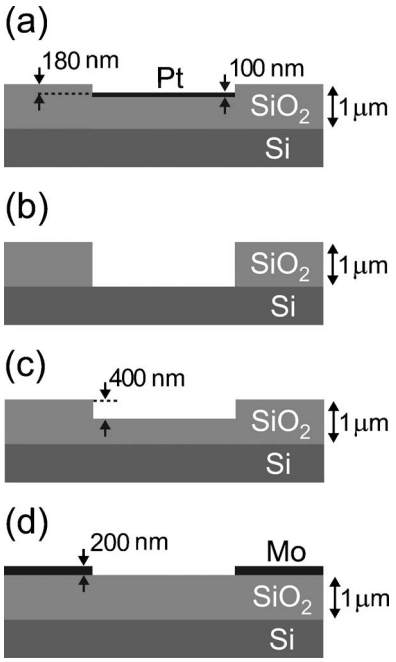

FIG. 2. Cross-section views of four types of substrates used in this study: type (a) platinum trench substrate, type (b) silicon trench substrate, type (c) silicon dioxide trench substrate, and type (d) molybdenum finger substrate.

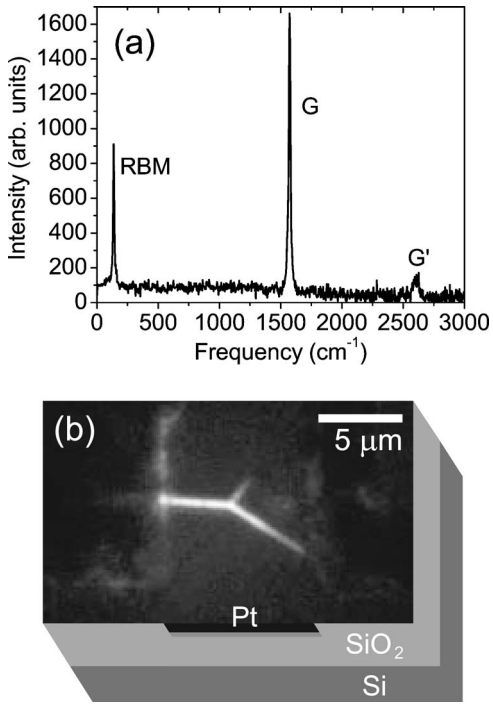

FIG. 3. Raman spectrum and image. (a) A typical Raman spectrum of an SWNT suspended over a trench etched in silicon dioxide with platinum recessed at the base of the trench. A background spectrum taken from a spot just off the nanotube was subtracted. (b) The corresponding Raman image of the nanotube generated by detecting the *G* band with global illumination. This nanotube forms a *Y* junction bundle with all segments visible.

quality. Similar methods, sometimes called "Ramanography" have been used in various applications in the past,[10–12] but their use in the nanotube material system, or individual nanotubes in particular, has not been reported, to our knowledge.

Nanotubes were grown by cold wall chemical vapor deposition on patterned substrates with nanoparticle catalysts and methane/hydrogen[13,14] or ethanol vapor/argon/hydrogen sources.[15] The catalyst consisted of electron beam deposited films of nominally 1 nm aluminum and 1 nm iron, which break up into nanoparticles upon heating in the reactor. A variety of samples were fabricated for two main reasons. First, the Raman imaging method is sensitive to the background scattered light, and so we wanted to establish that it worked in many situations. Second, nanotube manipulation is expected to depend on the geometry and the dielectric environment. Suspended nanotubes were therefore investigated on several different substrate types. All the samples also had nonsuspended nanotubes. The different types of samples had nanotubes suspended over platinum [type (a)], silicon [type (b)], and silicon dioxide [types (c) and (d)], as shown in Fig. 2. Samples were prepared using photolithography and electron beam lithography, wet and dry etching, electron-beam evaporation (Pt) and magnetron sputtering (Mo). No further processing was done after the growth of the nanotubes. The relevant dimensions for these samples are given in Fig. 2. On the substrate of type (b) the catalyst was deposited over the whole surface, while on all other substrates the catalyst film was patterned into widely spaced, 2 μm wide strips running perpendicular to the trenches using electron beam lithography.

III. RESULTS AND DISCUSSION

A. Imaging

Figure 3 shows the Raman spectrum of a suspended CNT on a substrate of type (a) along with its corresponding Raman image. Although spectra can be detected with a defocused spot (60 MW/m^2), spectra obtained with a focused spot (7 mW on a 2.5 μm spotsize, 1.4 GW/m^2) have a lower background level, and a stronger signal. The spectrum shows three features, a strong *G*-band peak at 1578 cm^{-1} and a radial breathing mode (RBM) at 137 cm^{-1} and a weaker and broader *G′*-band peak around 2615 cm^{-1}. The presence of a RBM implies a SWNT of diameter around 1.8 nm,[16–18] which is classified as semiconducting both according to its position (RBM frequency, laser frequency) on the Kataura plot[19] and the shape of the *G*-band peak.[20] The fact that the *G′* peak is observed with no visible *D*-band peak indicates good crystallinity and low disorder of the SWNT.[21] Raman spectra of all the nanotubes tested in this study exhibited *G* and *G′* peaks, though not all showed a RBM. The Raman image in Fig. 3(b) shows that the tube forms a *Y* junction and thus forms a bundle of two or more tubes. Interestingly, all legs of this *Y* junction are bright in the *G*-band image. It is important to note that this type of Raman imaging is chirality selective in that only the nanotubes which are resonant with the laser are imaged. Different species of nanotubes can therefore be imaged depending on the laser frequency used.

In general, the strength of Raman signals is greater for suspended nanotubes than for nanotubes lying on

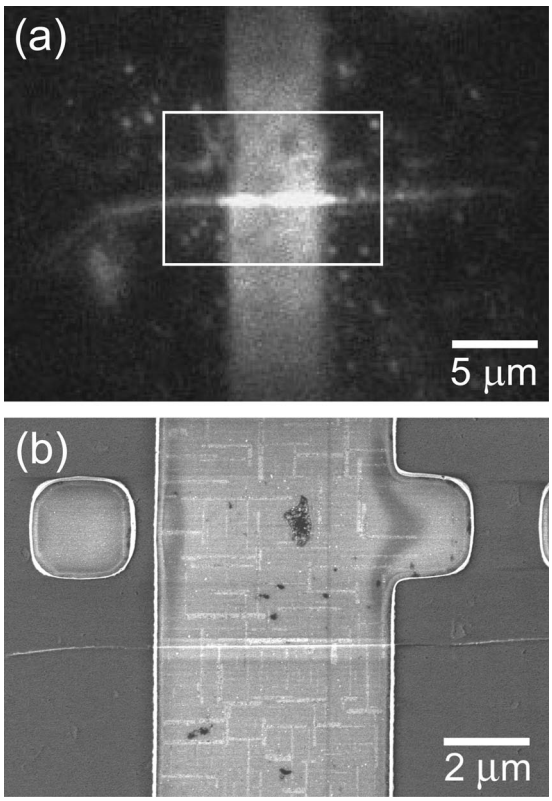

FIG. 4. (a) Raman image of a CNT suspended over a trench. The bright segment in the image corresponds to the suspended part of the tube. (b) A SEM image of the same CNT showing the suspended segment. The area imaged with the SEM is outlined by the white box in (a).

substrates.[22,23] The Raman image in Fig. 4(a) directly confirms this enhancement effect in a CNT on a substrate of type (b) which has both a suspended segment and parts lying flat on silicon dioxide. The suspended segment brightness is 1640 ± 200 (arbitrary units) above the background compared to 640 ± 100 for the nonsuspended parts, which corresponds to a 2.5 signal enhancement factor. This is a lower bound on the enhancement factor, because surface roughness produced by the presence of catalyst nanoparticles on the silicon dioxide inadvertently suspends some very short segments. Raman signals from suspended portions of nanotubes grown on substrates with patterned catalyst, in which the unsuspended parts lie flat on clean silicon dioxide, such as the one previously shown in Fig. 3(b), showed up to a tenfold signal enhancement.

Figure 4(b) is a SEM image of the CNT shown by Raman imaging in Fig. 4(a). The SEM image was taken in plan view from the area outlined by the white box in Fig. 4(a). The segment over the trench was also examined by SEM at various tilt angles to confirm that it was truly suspended. It is important to note that performing SEM observations on the CNT samples makes them difficult to use for subsequent Raman imaging. This is because a bright background develops on the sample surface in the region where the sample is exposed to the electron beam. This background likely stems from carbon deposition induced by the electron beam, and varies in intensity with magnification and with choice of observation voltage. Raman imaging thus shows, in a very direct way, that SEM observation is invasive as it changes the sample surface and therefore the nanotube environment.

Samples with high spectral background in the area of interest are unsuitable for Raman imaging. The background is particularly high in samples in which the catalyst is deposited over the whole sample surface, in some cases due to a high nanotube yield, in other cases, presumably due to graphitic coating on nanoparticles which have failed to extrude nanotubes. The samples best suited for this imaging method are those which have localized catalyst areas and isolated nanotubes.

B. Optical manipulation

Optically imaging CNTs is rapid and noninvasive and allows for the study of nanotube motion and manipulation. In fact, we observed that suspended CNTs are not static in the optical field, but rather they can easily be manipulated at moderate laser power. As we will now describe, we have used the laser to "push" suspended nanotubes so that they touch down on the surface and make contact locally and controllably. The manipulation process can be observed in real-time using the Raman imaging method.

In order to push the segment down onto the substrate surface the defocusing lens ($L1$) is removed so that the laser beam (20 mW on a 2.5 μm spotsize, 4 GW/m^2) is focused directly on the CNT. Very few nanotubes could be manipulated at 7 mW power, and no nanotubes were observed to change at power densities lower than this, even after focusing on the CNT for long periods of time. The dynamics of manipulation can be observed in real-time on the CCD with an integration time of 0.2 s per frame. Immediately after 20 mW excitation, a short, extremely bright, elongated segment is observed which, within a few seconds, disintegrates into a circular spot of decreased brightness. The defocusing lens is then reinserted to capture a postmanipulation Raman image. The manipulation of the tubes was tested on different types of substrates. On the sample of type (a), 11 suspended segments were tested and all 11 were permanently pushed down. On the sample of type (b), two suspended segments were tested and both were permanently pushed down. On the sample of type (c), 12 suspended segments were tested and of those three were permanently pushed down onto the substrate while the other nine remained unchanged. Finally, on the sample of type (d), seven suspended segments were tested and of those three were permanently pushed down while the other four remained unchanged. Before drawing conclusions from these numbers, it must be recognized that each sample had a different density of nanotubes, and likely also a different diameter distribution and degree of bundling.

Figure 5 shows example of Raman images of CNTs before and after optical manipulation. The leftmost panels show suspended CNT segments before manipulation and the rightmost panels show the effect of manipulation. Figures 5(a) and 5(b) show manipulation on a sample of type (d), for a CNT suspended from molybdenum mesa to molybdenum mesa. Figures 5(c) and 5(d) show the same effect on a platinum substrate [type (a)], for a CNT suspended from silicon

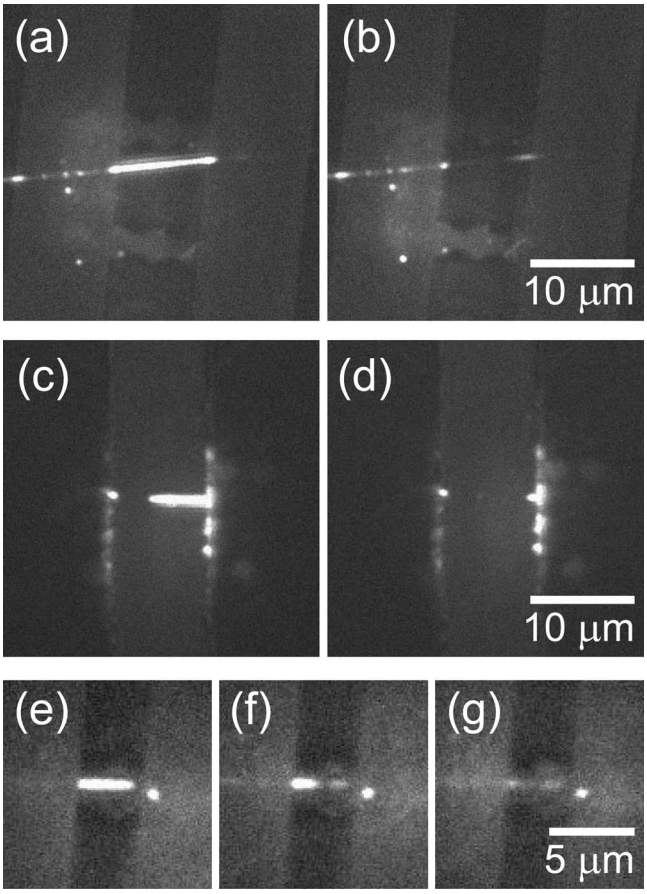

FIG. 5. Optical manipulation of individual suspended CNTs. A nanotube suspended over silicon dioxide from molybdenum mesas (a) before and (b) after manipulation. A nanotube suspended over recessed platinum fingers from silicon dioxide mesas (c) before and (d) after manipulation. A nanotube suspended over silicon dioxide from molybdenum mesas (e) before manipulation, (f) after a first manipulation step, and (g) after a second manipulation step.

dioxide mesas over a recessed platinum finger. In some cases the manipulation was done in two or more separate steps, as shown in the lower panels (e), (f), and (g) of Fig. 5, for a CNT on a sample of type (d). In the first step, the laser is focused close to the right end of the suspended segment and pushes down only a part of the suspended CNT. In the second step the laser is focused on the remaining bright, suspended segment and pushes the rest of the CNT down onto the substrate surface.

To confirm that the manipulated CNTs touched down onto the substrate surface, many manipulated nanotubes were examined by SEM immediately after manipulation. Figure 6(a) shows one example of a formerly uniformly bright nanotube after separately manipulating two suspended segments. To increase the viewing area, two separate fields of view are overlaid to form this image. In this example the type (b) sample has a thick silicon dioxide layer (dark) which has been etched into trenches with silicon at the base (light). The CNT can be seen running diagonally and has been pushed down into two adjoining trenches. Figure 6(b) shows SEM images of the same area. The full figure was taken in plan view, while the higher magnification insets were taken at a

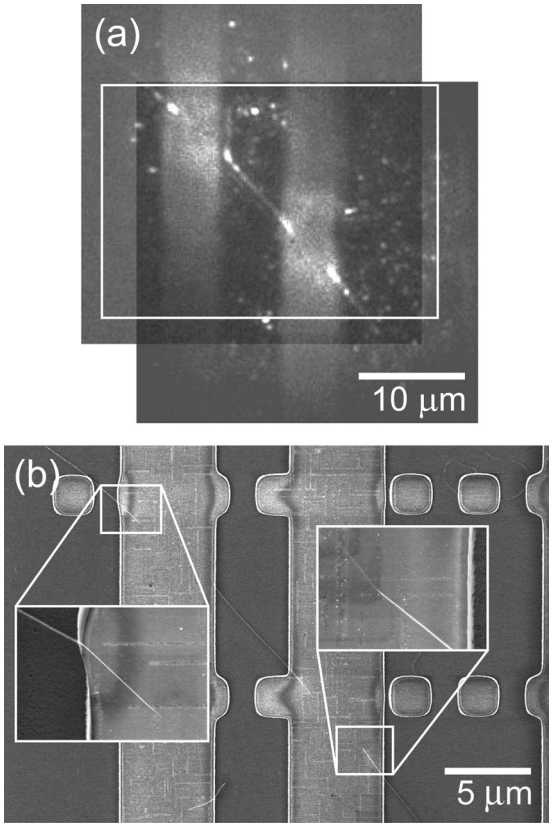

FIG. 6. Detailed images of a nanotube after manipulation. (a) Two overlaid Raman images showing a nanotube that was initially suspended and subsequently pushed down. The substrate is silicon with 1 μm thick silicon dioxide (dark) which has been etched into trenches with silicon at the base (light). (b) SEM images of the same area. The large image was taken in plan view, while the higher magnification insets were taken at a 30° tilt. The large area imaged with the SEM is outlined by the white box in (a).

30° angle. The images confirm that the nanotube has been pushed down by the focused laser beam onto the silicon, but still has tilted suspended segments near the trench walls. There is a one-to-one correspondence between the short suspended segments near the edges of the trench, which are visible in the SEM image, and the short bright segments in the same location in the Raman image. This correspondence again illustrates that a suspended nanotube is substantially brighter in Raman than one on the surface.

C. Manipulation mechanism

Having shown several examples of optical manipulation, we next discuss the relevant physical mechanisms. There are several mechanisms through which the nanotube can make contact with the substrate, and they may be classified into those which arise directly from the photon field, and those for which the substrate itself plays an important role. Laser induced heating may cause thermal vibrations large enough for the nanotube to contact the substrate.[24] Purely optical forces, either from photon momentum transfer, or from the induced dipole gradient force may also be important. Finally,

TABLE I. Possible mechanisms of nanotube manipulation and their corresponding magnitude. $S=4$ GW/m^2 is the optical power density, $A'=10^{-16}$ m^2 is the optical absorption area, E is the peak electric field given by $E=\sqrt{S/\varepsilon_0 c}$, p is the dipole moment such that $p=\alpha E$, where α is the static polarizability in *Systeme International* (SI) units, $L'=2.5$ μm is the laser spot diameter, q is the charge, $r=200$ nm is the separation between charges, σ is the thermal vibration amplitude, $L=5$ μm is the length of the tube, $d=1.8$ nm is the nanotube diameter, $Y=1$ T Pa is the Young's modulus from Ref. 24, T is the temperature, and $\kappa=3\times10^3$ W/m K is the thermal conductivity from Ref. 43. The relationship between α and the extrapolated polarizability per unit length $\alpha'\sim2\times10^{-17}$ m^2 from Ref. 37 is $\alpha=4\pi\varepsilon_0\alpha' L'$.

Physical mechanism		Mathematical equation	Magnitude
Optical	Momentum force	$F=\frac{SA'}{c}$	$F=1$ fN
	Gradient force	$F=\lvert(\vec{p}\cdot\nabla)\vec{E}\rvert\cong\frac{2\alpha E^2}{L'}$	$F=6$ fN
Electrostatic	Monopole force	$F=\frac{1}{4\pi\varepsilon_0}\frac{q^2}{r^2}$	$F=6$ fN/charge^2
	Dipole force	$F=\frac{1}{4\pi\varepsilon_0}\frac{p^2}{r^4}=\frac{1}{4\pi\varepsilon_0}\frac{\alpha^2E^2}{r^4}$	$F=4$ fN
Thermal	Vibration amplitude	$\Delta\sigma=\sqrt{\frac{k_B L^3}{12\pi d^4 YT}}\Delta T$ $\Delta T=\frac{2L}{\kappa\pi d^2}SA'$	$\Delta\sigma=18$ nm

electrostatic forces may act through the substrate either via polarization or charging.

The magnitudes of forces required to manipulate nanotubes can be estimated. A nanotube suspended over a trench may be modeled either as a suspended elastic string clamped at both ends or as a stiff supported beam. It has been proposed that the elastic string model is applicable to taut nanotubes whereas nanotubes suspended with a certain amount of slack are more accurately modeled as stiff supported beams.[27,28] Slack here means that the nanotube has a suspended length greater than the distance between anchoring points. A taut nanotube will stretch appreciably when subjected to forces on the order of 1 nN.[29] A taut SWNT can sustain strains up to 5% of its length with an average breaking strength of 30 GPa,[30,31] corresponding to a force of order 100 nN. However, it has been shown that a slack SWNT requires much less force to bend.[25] When a nanotube is slack it bends without stretching and it can therefore be modeled as a stiff cantilever clamped at one end. We calculated the force needed to displace a nanotube cantilever, which bends with a linear force constant. A 5 μm long nanotube of 1.8 nm diameter requires a force of 1 fN to displace by 100 nm.[26]

The various mechanisms and forces that act on a suspended nanotube in an optical field are listed in Table I. The magnitude of each is estimated for an example case of a single SWNT of 1.8 nm diameter, suspended over a length of 5 μm at a height of $h=100$ nm above the substrate surface. We took the laser power to be 20 mW focused to a 2.5 μm diameter spot. An estimated optical absorption cross section of $\sim10^2$ m^2/molCarbon was used to calculate an effective absorption area of 10^{-16} m^2.[32]

First, thermally induced vibration due to laser heating could cause a nanotube to make contact with the surface if the amplitude of vibration is sufficiently large. Assuming that all the absorbed photons are converted to heat, and that all the heat loss is through the ends of the nanotube, we estimate a temperature increase of 167 °C for a vibration amplitude of 90 nm, which is 18 nm higher than at room temperature.[33] However, SEM observation of our nanotubes at room temperature did not reveal any oscillations greater than ~10 nm. Furthermore, other experiments indicate that nanotubes excited to these power densities actually do not heat up nearly as much as the above estimate would suggest[34] and most nanotubes do not exhibit any measurable vibration.[24] We therefore discount this as the mechanism in our case.

Optical fields can also manipulate small molecules such as SWNTs either through absorption and scattering or through the polarizability. The change in momentum of absorbed or scattered photons exerts a force which depends on the optical absorption or scattering cross section and the power density. In the example case, the momentum transfer leads to a 1 fN force. In addition, an optical gradient force arises from the polarizability of the nanotube. This force has

been used to trap carbon nanotubes in solution.[35,36] The electric field from the laser induces optical transition dipoles along the nanotube axis which then interact with the gradient of the electric field. The magnitude of the force can be calculated using the reported static polarizability,[37] and by approximating the field gradient as decreasing linearly from that determined by the power density to zero over a distance equivalent to the spot radius. Using this method the estimated optical gradient force is 6 fN.

Separate from purely optical forces, electrostatic forces acting on nanotubes can be important and have been used, for example, to locate nanotubes between electrodes using electrophoresis,[38] to align nanotubes during growth,[39] or to change the resonance frequency of a suspended nanotube.[28] Close to the substrate, electrostatic interactions with the substrate will overwhelm the purely photon field related forces. For a conducting substrate, the polarized nanotube will interact with an induced image dipole at a distance r, where $r=2h$. For the example case, using static polarizability, this force was calculated to be 4 fN, which is comparable to the optical forces. For poorly conducting substrates the image charge force would be significantly weaker.

In addition to polarization, localized charge monopoles may be generated. For example, a donor or acceptor impurity in the nanotube may be ionized with the mobile elementary charge escaping from the nanotube to the substrate or to the interface. Static point charges may also be photoinduced in the oxide or interfaces.[40,41] A single elementary charge and its image charge in the substrate give rise to a 6 fN force, which is as large as the optical force. Of course, more complicated electrostatic interactions, such as dipole monopole are possible. If charges are induced separately on the substrate and the nanotube, even repulsive interactions are also possible.

Based on the calculation of forces acting on a SWNT in an optical field in the example case, both the optical and electrostatic mechanisms give rise to forces on the order of femto-Newtons. Comparing this value with the estimated of magnitude force necessary to manipulate a nanotube it is clear that the forces are large enough to push a slack SWNT, but not strong enough to stretch or a break taut nanotube a nanotube. The calculation results are supported by the experimental observation that only a fraction of the nanotubes tested, presumably the ones with a sufficient amount of slack, could be effectively manipulated.

Based on the scaling relationships in Table I, for large separation between the suspended part of the nanotube and the substrate optical forces are the strongest, while electrostatic forces dominate at small separation. Since the electrostatic forces diverge as the distance between the charges or dipoles decreases, it is conceivable that these forces could stretch and even break the SWNT if the nanotube gets sufficiently close to the substrate. SEM analysis of the manipulated nanotubes revealed that some of the CNTs were indeed broken, providing evidence for forces of this magnitude. It is also important to note that throughout Table I we have used the static polarizability to estimate the dipole moment. This a poor approximation at optical frequencies, especially given that Raman scattering from CNTs is a resonant process and at resonance the polarizability of a nanotube should be strongly enhanced.[42] Therefore, we expect the gradient force and the electrostatic dipole forces to increase considerably since they scale with the square and the fourth power of polarizability, respectively. The optical momentum force also depends on the resonance conditions through the absorption/scattering cross section. The effect of the power density and resonant conditions on the monopole mechanism is unclear as there is no complete picture of the process by which the charge would be generated.

IV. CONCLUSIONS

In conclusion, we have demonstrated a method for global Raman imaging of suspended CNTs which is capable of real-time observation. This type of imaging can also be generalized to other Raman bands, such as the RBM, or to infrared photoluminescence peaks. We have also shown that suspended CNTs can be optically manipulated with a focused laser beam, and explored the physical processes that may be involved. The observation that suspended nanotubes are not static in the optical field is very important as it shows that optical measurement changes the state of the nanotube. The capability to select and manipulate individual CNTs should enable more controlled fabrication of networks of nanotubes and other complex structures. Such methods are immediately practical for "wiring up" of suspended nanotubes by forcing them onto metallic electrical contacts.

ACKNOWLEDGMENTS

We gratefully acknowledge J. Bond for help with chemical vapor deposition (CVD) growth, L. Tay for advice on Raman spectroscopy and the NRC Nanofabrication group for assistance with substrate preparation. We also thank Robin Williams for helpful comments. High performance edge filters were generously supplied by Iridian Spectral Technologies. We are grateful for funding provided by a grant from JST-CREST, as a part of the "Nano-factory" project led by Y. Homma.

[1] S. Iijima, Nature (London) **354**, 56 (1991).

[2] S. Iijima and T. Ichihashi, Nature (London) **363**, 603 (1993).

[3] D. S. Bethune, C. H. Klang, M. S. de Vries, G. Gorman, R. Savoy, J. Vazquez, and R. Beyers, Nature (London) **363**, 605 (1993).

[4] S. K. Doorn, L. Zheng, M. J. O'Connell, Y. Zhu, S. Huang, and J. Liu, J. Phys. Chem. B **109**, 3751 (2005).

[5] S. K. Doorn, M. J. O'Connell, L. Zheng, Y. Zhu, S. Huang, and J. Liu, Phys. Rev. Lett. **94**, 016802 (2005).

[6] A. Hartschuh, E. J. Sanchez, X. S. Xie, and L. Novotny, Phys.

Rev. Lett. **90**, 095503 (2003).
[7] N. Anderson, A. Hartschuh, S. Cronin, and L. Novotny, J. Am. Chem. Soc. **127**, 2533 (2005).
[8] D. A. Tsyboulski, S. M. Bachilo, and R. B. Weisman, Nano Lett. **5**, 975 (2005).
[9] M. S. Dresselhaus, G. Dresselhaus, R. Saito, and A. Jorio, Phys. Rep. **409**, 47 (2005).
[10] P. J. Treado, I. W. Levin, and E. N. Lewis, Appl. Spectrosc. **46**, 1211 (1992).
[11] G. J. Puppels, M. Grond, and J. Greve, Appl. Spectrosc. **47**, 1258 (1993).
[12] N. M. Sijtsema, S. D. Wouters, C. J. De Grauw, C. Otto, and J. Greve, Appl. Spectrosc. **52**, 348 (1998).
[13] P. Finnie, J. Bardwell, I. Tsandev, M. Tomlinson, M. Beaulieu, J. Fraser, and J. Lefebvre, J. Vac. Sci. Technol. A **22**, 747 (2004).
[14] P. Finnie, A. Li-Pook-Than, J. Lefebvre, and D. G. Austing (unpublished).
[15] S. Chiashi, Y. Murakami, Y. Miyauchi, and S. Maruyama, Chem. Phys. Lett. **386**, 89 (2004).
[16] A. Jorio, R. Saito, J. H. Hafner, C. M. Lieber, M. Hunter, T. McClure, G. Dresselhaus, and M. S. Dresselhaus, Phys. Rev. Lett. **86**, 1118 (2001).
[17] S. M. Bachilo, M. S. Strano, C. Kittrell, R. H. Hauge, R. E. Smalley, and R. B. Weisman, Science **298**, 2361 (2002).
[18] J. C. Meyer, M. Paillet, T. Michel, A. Moreac, A. Neumann, G. S. Duesberg, S. Roth, and J.-L. Sauvajol, Phys. Rev. Lett. **95**, 217401 (2005).
[19] H. Kataura, Y. Kumazawa, Y. Maniwa, I. Umezu, S. Suzuki, Y. Ohtsuka, and Y. Achiba, Synth. Met. **103**, 2555 (1999).
[20] A. Jorio, A. G. Souza Filho, G. Dresselhaus, M. S. Dresselhaus, A. K. Swan, M. S. Unlu, B. Goldberg, M. A. Pimenta, J. H. Hafner, C. M. Lieber, and R. Saito, Phys. Rev. B **65**, 155412 (2002).
[21] A. G. Souza Filho, A. Jorio, A. K. Swan, M. S. Unlu, B. B. Goldberg, R. Saito, J. H. Hafner, C. M. Lieber, M. A. Pimenta, G. Dresselhaus, and M. S. Dresselhaus, Phys. Rev. B **65**, 085417 (2002).
[22] Y. Kobayashi, T. Yamashita, Y. Ueno, O. Niwa, Y. Homma, and T. Ogino, Chem. Phys. Lett. **386**, 153 (2004).
[23] H. Son, Y. Hori, S. G. Chou, D. Nezich, Ge. G. Samsonidze, G. Dresselhaus, M. S. Dresselhaus, and E. B. Barros, Appl. Phys. Lett. **85**, 4744 (2004).
[24] B. Babic, J. Furer, S. Sahoo, Sh. Farhangfar, and C. Schonenberger, Nano Lett. **3**, 1577 (2003).
[25] E. D. Minot, Y. Yaish, V. Sazonova, J.-Y. Park, M. Brink, and P. L. McEuen, Phys. Rev. Lett. **90**, 156401 (2003).
[26] E. W. Wong, P. E. Sheehan, and C. M. Lieber, Science **277**, 1971 (1997).
[27] D. A. Walters, L. M. Ericson, M. J. Casavant, J. Liu, D. T. Colbert, K. A. Smith, and R. E. Smalley, Appl. Phys. Lett. **74**, 3803 (1999).
[28] V. Sazonova, Y. Yaish, H. Ustunel, D. Roundy, T. A. Arias, and P. L. McEuen, Nature (London) **431**, 284 (2004).
[29] T. W. Tombler, C. Zhou, L. Alexseyev, J. Kong, H. Dai, C. S. Jayanthi, M. Tang, and S.-Y. Wu, Nature (London) **405**, 769 (2000).
[30] M. B. Nardelli, B. I. Yakobson, and J. Bernholc, Phys. Rev. Lett. **81**, 4656 (1998).
[31] M.-F. Yu, B. S. Files, S. Arepalli, and R. S. Ruoff, Phys. Rev. Lett. **84**, 5552 (2000).
[32] M. F. Islam, D. E. Milkie, C. L. Kane, A. G. Yodh, and J. M. Kikkawa, Phys. Rev. Lett. **93**, 037404 (2004).
[33] S. Sapmaz, Ya. M. Blanter, L. Gurevich, and H. S. J. van der Zant, Phys. Rev. B **67**, 235414 (2003).
[34] H. Son, Y. Hori, S. G. Chou, D. Nezich, Ge. G. Samsonidze, G. Dresselhaus, M. S. Dresselhaus, and E. B. Barros, Appl. Phys. Lett. **85**, 4744 (2004).
[35] J. Plewa, E. Tanner, D. M. Mueth, and D. G. Grier, Opt. Express **12**, 1978 (2004).
[36] S. Tan, H. A. Lopez, C. W. Cai, and Y. Zhang, Nano Lett. **4**, 1415 (2004).
[37] L. X. Benedict, S. G. Louie, and M. L. Cohen, Phys. Rev. B **52**, 8541 (1999).
[38] K. Yamamoto, S. Akita, and Y. Nakayama, Jpn. J. Appl. Phys., Part 2 **35**, L917 (1996).
[39] Y. Zhang, A. Chang, J. Cao, Q. Wang, W. Kim, Y. Li, N. Morris, E. Yenilmez, J. Kong, and H. Dai, Appl. Phys. Lett. **79**, 3155 (2001).
[40] E. T. Enikov and A. Palaria, Nanotechnology **15**, 1211 (2004).
[41] C. H. Ben-Porat, O. Cherniavskaya, L. Brus, K.-S. Cho, and C. B. Murray, J. Phys. Chem. A **108**, 7814 (2004).
[42] F. Torrens, Nanotechnology **15**, S259 (2004).
[43] J. Hone, M. Whitney, C. Piskoti, and A. Zettl, Phys. Rev. B **59**, R2514 (1999).